High-fidelity method for a single-step *N*-bit Toffoli gate in trapped ions

Juan Diego Arias Espinoza[1], Koen Groenland[2], Matteo Mazzanti[1], Kareljan Schoutens[2,3] and Rene Gerritsma[1]

[1]*Van der Waals-Zeeman Institute, Institute of Physics, University of Amsterdam, 1098 XH Amsterdam, Netherlands*
[2]*QuSoft, Science Park 123, 1098 XG Amsterdam, Netherlands*
[3]*Institute for Theoretical Physics, Institute of Physics, University of Amsterdam, Science Park 904, 1098 XH Amsterdam, Netherlands*

Conditional multiqubit gates are a key component for elaborate quantum algorithms. In a recent work, Rasmussen *et al.* [Phys. Rev. A **101**, 022308 (2020)] proposed an efficient single-step method for a prototypical multiqubit gate, a Toffoli gate, based on a combination of Ising interactions between control qubits and an appropriate driving field on a target qubit. Trapped ions are a natural platform to implement this method, since Ising interactions mediated by phonons have been demonstrated in increasingly large ion crystals. However, the simultaneous application of these interactions and the driving field required for the gate results in undesired entanglement between the qubits and the motion of the ions, reducing the gate fidelity. In this work, we propose a solution based on adiabatic switching of these phonon-mediated Ising interactions. We study the effects of imperfect ground-state cooling and use spin-echo techniques to undo unwanted phase accumulation in the achievable fidelities. For gates coupling to all axial modes of a linear crystal, we calculate high-fidelity ($>99\%$) *N*-qubit rotations with $N = 3$–7 ions cooled to their ground state of motion and a gate time below 1 ms. Finally, we study the effect of laser intensity fluctuations and find that the proposed gate requires intensity stabilization with subpercentage noise levels. The high fidelities obtained also for large crystals could make the gate competitive with gate-decomposed, multistep variants of the *N*-qubit Toffoli gate, at the expense of requiring ground-state cooling of the ion crystal.

I. INTRODUCTION

Quantum computers promise dramatic speedups in a variety of disciplines [1–5] but remain challenging to scale up in practice. A major obstacle to executing elaborate quantum algorithms is the need for gates that act conditionally on a large number of qubits. The prototypical example of such a gate is the *N*-qubit Toffoli gate, which flips a single "target" qubit if and only if all $N - 1$ "control" qubits are in state $|1\rangle$. Even though quantum devices with over 50 qubits have been reported [6,7], the largest Toffoli gate ever performed is, to our best knowledge, the case $N = 4$ [8]. This gap is surprising because Toffoli gates (or equivalents) are essential ingredients of many basic computation steps, such as elementary arithmetic [9–11], error correction [12], and the Grover diffusion operator [13].

Two different strategies exist to implement Toffoli gates. The first consists of decomposing a single *N*-qubit Toffoli gate into a circuit consisting of one- and two-qubit gates [14–16] or multiqubit gates, such as the Mølmer-Sørensen gate in trapped ions [17–19]. The second approach is to perform the gate in a single step using interactions that are native to the specific platform [20–23]. In particular, a recent proposal [23] has demonstrated that, by exploiting systems with an all-to-all Ising interaction in combination with a drive field on a single target qubit, an *i*-Toffoli gate can be implemented. This gate differs from the regular Toffoli gate only by a phase $+i$ on the target states which, if required, can be removed at the cost of a single ancilla.

Trapped ions are a natural candidate to implement this proposal because intrinsic Ising interactions have been demonstrated in increasingly large ion crystals [6,17,24–26]. Moreover, quantum operations have been demonstrated [27,28] with fidelities higher than 99.9%. Ising interactions generally arise from qubit-phonon couplings $\hat{H}_\text{q-ph}$ generated from state-dependent laser-induced forces on the ions. Combining this mechanism with the driving field $\hat{H}_\text{drive}$ required for an *i*-Toffoli gate poses a problem because the processes do not commute i.e., $[\hat{H}_\text{q-ph}, \hat{H}_\text{drive}] \neq 0$. As a result, the qubit states and the motion of the ions remain entangled at the end of the gate sequence, which leads to fidelity loss. This effect could be mitigated by restricting the strength of the spin-phonon coupling such that the phonons are only virtually excited [26,29]. However, limiting the strength of the Ising interactions leads to undesirably long gate times.

In this work, we show that this residual qubit-phonon entanglement can be suppressed by adiabatic ramping of $\hat{H}_\text{q-ph}$. In this way, the *i*-Toffoli gate operates on the dressed eigenstates of $\hat{H}_\text{q-ph}$, which are adiabatically connected to the Fock eigenstates of the noninteracting system. The benefit of this approach is that the effective Ising interaction strength does not have to be limited to the regime of virtual phonon excitation. We show that high-fidelity $\bar{F} > 99\%$, single-step *i*-Toffoli gates should be possible with up to seven ions at gate times $\approx 600~\mu$s, assuming ground-state-cooled crystals and sufficient suppression of laser intensity fluctuations.
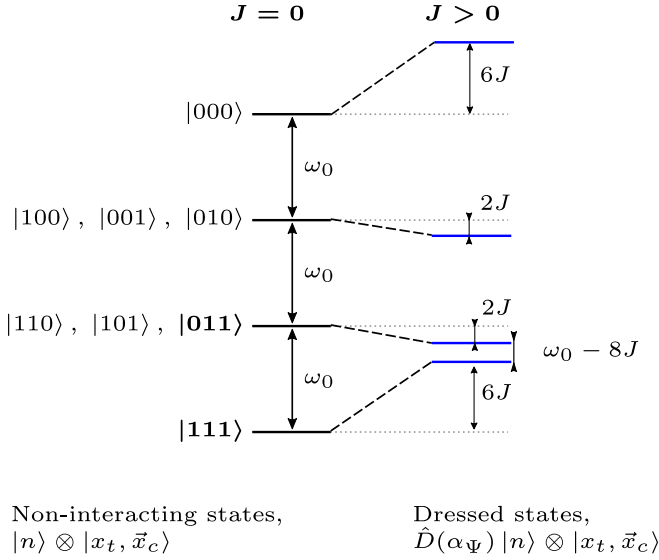
FIG. 1. Energies of noninteracting eigenstates ($J = 0$) and interacting (dressed) states ($J > 0$). The two target states $|111\rangle$, $|011\rangle$ are highlighted. Because their energy gap is unique, an appropriate drive field can couple the states resonantly.

We start in Sec. II with the derivation of the model for a N-qubit i-Toffoli gate for a system of trapped ions and introduce our proposal for adiabatic preparation of dressed states. In Sec. III we analyze the results of numerical simulations for a linear three-ion crystal and consider the role of inhomogeneous Ising interactions mediated by multiple phonon modes. We discuss the implementation of a method based on multifrequency laser fields [30] to eliminate undesired phases originating from these inhomogeneous interactions. Finally, in Sec. IV we calculate the fidelities for 3–9 qubits gates and discuss sources of errors and ways to mitigate them. We also consider the effects of imperfect ground-state cooling.

II. MODEL OF N-QUBIT TOFFOLI GATE IN TRAPPED IONS

A. Single-step N-qubit i-Toffoli gate

Briefly, the proposal [23] requires qubits coupled via an Ising interaction of the form $\hat{H}_{\text{Ising}} = \sum_{ij}^{N} J^{(i,j)} \hat{\sigma}_z^{(i)} \hat{\sigma}_z^{(j)}$ with $\hat{\sigma}_z^{(i)}$ being the Pauli matrix acting on ion i, and $J^{(i,j)}$ being the strength of the interaction field.[1] Including a drive field of frequency ω_g with strength g acting on the target qubit, $\hat{H}_{\text{drive}} = g \hat{\sigma}_x^{(t)} \cos(\omega_g t)$, and the energy of the noninteracting qubits, $\hat{H}_0 = \omega_0/2 \sum_i \hat{\sigma}_z^{(i)}$, a simple Hamiltonian is obtained:

$$\hat{H}_T = -\frac{\nu}{2} \sum_i \hat{\sigma}_z^{(i)} + \sum_{i \neq j} J^{(i,j)} \hat{\sigma}_z^{(i)} \hat{\sigma}_z^{(j)} + \frac{g}{2} \hat{\sigma}_x^{(t)}, \quad (1)$$

where we transformed into the interaction picture with respect to ω_g, using $\hat{U} = \exp(U^{-i\omega_g \sigma_z t/2})$. We also define $\nu = \omega_g - \omega_0$ with ω_0 being the energy spacing between qubit states (or

eigenstates of $\hat{\sigma}_z$). These eigenstates and their energies (Fig. 1) can be labeled as $|x_t, \vec{x}_c\rangle$ and $E_{|x_t, \vec{x}_c\rangle}$ with x_t describing the state of the target qubit and $\vec{x}_c$ being the string describing the state of the control qubits. In particular, the two target states are labeled as $|0, 1^{N_c}\rangle$, $|1, 1^{N_c}\rangle$, where N_c corresponds to the number of control qubits.

The driving field frequency (ω_g) is chosen such that it resonantly couples these two states, i.e., $\Delta_{1^{N_c}} = E_{|0,1^{N_c}\rangle} - E_{|1,1^{N_c}\rangle} = \omega_g$. According to Eq. (1) the energy gap for any pair of states with equal control bits can be written as

$$\Delta_{\vec{x}_c} = 4 \sum_{i=1}^{N_c} J^{(t,i)} (-1)^{x_i} + \omega_0, \quad (2)$$

where x_i denotes the state of the ith control qubit. The resonant condition becomes then $\nu = 4 \sum_{i=1}^{N_c} J^{(t,i)} (-1)^{x_i}$, which for the target states implies $\nu = -4 \sum_{i=1}^{N_c} J^{(t,i)}$.

Evolution under the Hamiltonian of Eq. (1) for a gate time $\tau_g = \pi/g$ leads to the desired i-Toffoli gate. To prevent accumulation of unwanted dynamical phases during the gate, timing restrictions can be considered, or an echo pulse can be applied. Both will be discussed later in this text.

B. Implementation in trapped ions

To achieve the required Ising interaction in trapped ions, a qubit state-dependent force is generated with two noncopropagating bichromatic lasers with beatnote frequency μ, which excites phonons in the ion crystal. For a homogenous laser field extending over the full ion crystal, the laser-ion interaction Hamiltonian is $\hat{H}_{\text{q-ph}} = \sum_i F_i \exp(i\vec{k} \cdot \hat{\vec{r}}^{(i)}) + \text{H.c.}$ Here $F_i = (\Omega/2) e^{-i\mu t} \hat{\sigma}_z^{(i)}$ is a state-dependent interaction [2] with Ω being the interaction strength, $\vec{k}$ the resulting wave vector of the interfering laser fields, and $\hat{\vec{r}}^{(i)}$ the position operator of ion i. With $\vec{k} \cdot \hat{\vec{r}}^{(i)} = \sum_m \eta_m^{(i)} (\hat{a}_m^\dagger + \hat{a}_m)$ the Hamiltonian can be written as

$$\hat{H}_{\text{q-ph}} = \frac{\Omega}{2} \sum_i \left(e^{i \sum_m \eta_m^{(i)} (\hat{a}_m^\dagger + \hat{a}_m) - i\mu t} + \text{H.c.} \right) \hat{\sigma}_z^{(i)}, \quad (3)$$

where the creation and annihilation operators for the mth phonon mode are denoted by $\hat{a}_m^\dagger$ and $\hat{a}_m$, respectively. The Lamb-Dicke parameter $\eta_m^{(i)}$ is scaled with the motion amplitude of the ith ion on the mth phonon mode ($\vec{b}_m^{(i)}$), i.e., $\eta_m^{(i)} = \vec{b}_m^{(i)} \cdot \vec{k} \sqrt{\hbar/(2M\omega_m)}$ with M being the ion mass and ω_m the phonon-mode frequency.

By including again the drive field ($\hat{H}_{\text{drive}}$) and the energy of the noninteracting system ($\hat{H}_0$), the total Hamiltonian in the interaction picture of ω_g becomes:

$$\hat{H}_T = -\frac{\nu}{2} \sum_i \hat{\sigma}_z^{(i)} + \sum_m \omega_m \hat{a}_m^\dagger \hat{a}_m$$

$$+ \frac{\Omega}{2} \sum_i \left(e^{i \sum_m \eta_m^{(i)} (\hat{a}_m^\dagger + \hat{a}_m) - i\mu t} + \text{H.c.} \right) \hat{\sigma}_z^{(i)} + \frac{g}{2} \hat{\sigma}_x^{(t)}, \quad (4)$$

which includes a new (second) term for the motional energy of the system. Now the eigenstates of the noninteracting system

---

[1] We define $\hbar = 1$ and thus omit it from all the Hamiltonians in this text.

[2] The dependence on the qubit state arises from a differential Stark shift set by the proper choice of laser polarizations [24].

have the form $|\Psi\rangle = |\Phi\rangle \otimes |x_t, \vec{x}_c\rangle$, with $|\Phi\rangle = \bigotimes_m |n_m\rangle$ the motional wave function of the system in the Fock space of the m phonon modes of the crystal. For this system we define the target states for the i-Toffoli gate as those corresponding to an ion crystal cooled to its ground state, that is, the two target states are $|\Psi_1\rangle = \bigotimes_m |n_m = 0\rangle \otimes |1, \vec{x}_c\rangle$ and $|\Psi_0\rangle = \bigotimes_m |n_m = 0\rangle \otimes |0, \vec{x}_c\rangle$.[3]

Next, we simplify this Hamiltonian by going into the interaction picture of the phonon mode frequencies with the transformation $\hat{U} = \exp(-it \sum_m \omega_m \hat{a}_m^\dagger \hat{a}_m)$:

$$
\tilde{H}_T = -\frac{\nu}{2} \sum_i \hat{\sigma}_z^{(i)} + \frac{\Omega}{2} \sum_i \left(e^{i \sum_m \eta_m^{(i)}(\hat{a}_m^\dagger e^{i\omega_m t} + \text{H.c.}) - i\mu t} \right.
$$
$$
\left. + \text{H.c.} \right) \hat{\sigma}_z^{(i)} + \frac{g}{2} \hat{\sigma}_x^{(t)}, \tag{5}
$$

where high-frequency terms ($2\omega_m$) were ignored. We now consider a system within the Lamb-Dicke limit and transform the Hamiltonian into a new interaction picture with respect to $\delta_m = \mu - \omega_m$ using $\hat{U} = \exp(-it \sum_m \delta_m \hat{a}_m^\dagger \hat{a}_m)$:

$$
\tilde{H}_{T,mm} = -\frac{\nu}{2} \sum_i \hat{\sigma}_z^{(i)} + \frac{i\Omega}{2} \sum_m \sum_i \left(\hat{a}_m^\dagger - \hat{a}_m \right) \eta_m^{(i)} \hat{\sigma}_z^{(i)}
$$
$$
- \sum_m \delta_m \hat{a}_m^\dagger \hat{a}_m + \frac{g}{2} \hat{\sigma}_x^{(t)}. \tag{6}
$$

Here we have used the rotating wave approximation and ignore frequencies higher than $|\delta_s|$.

To recover a Hamiltonian having the desired Ising interaction as in Eq. (1), we apply a Lang-Firsov transformation [31–33] to introduce a dressed-state picture of qubits entangled with phonon modes of the crystal. The transformation, $\hat{U}_I = \exp[-i \sum_{i,m} \alpha_m^{(i)}(\hat{a}_m^\dagger + \hat{a}_m)]$, with $\alpha_m^{(i)} = (\Omega \eta_m^{(i)}/2\delta_m)\hat{\sigma}_z^{(i)}$, has the form of a displacement operator that displaces the state of the system in phase space by a state dependent magnitude of $\alpha_{m,\Psi} = \sum_i \alpha_m^{(i)}$. The result of the transformation is

$$
\tilde{H}_{T,I} = \hat{U}_I^\dagger \tilde{H}_{T,sm} \hat{U}_I = -\frac{\nu}{2} \sum_i \hat{\sigma}_z^{(i)} + \sum_{i \neq j} J^{(i,j)} \hat{\sigma}_z^{(i)} \hat{\sigma}_z^{(j)}
$$
$$
- \sum_m \delta_m \hat{a}_m^\dagger \hat{a}_m + \frac{\tilde{g}}{2} \tilde{\sigma}_x^{(t)}, \tag{7}
$$

with $J^{(i,j)} = \Omega^2 \sum_m \eta_m^{(i)} \eta_m^{(j)}/4\delta_m$, a corrected drive strength $\tilde{g}$, and a transformed drive term $\tilde{\sigma}_x^{(t)} = \hat{U}_I^\dagger \hat{\sigma}_x^{(t)} \hat{U}_I$. Because the drive and the Ising terms do not commute, this transformation introduces a term $\propto \alpha_m^{(t)} \hat{\sigma}_y^{(t)}$ which couples the drive to ion motion and can cause a gate error $\propto \alpha_m^{(t)}$. For weak (virtual) phonon excitation, $\alpha_\Psi \ll 1$, such that $\tilde{\sigma}_x^{(t)} \approx \hat{\sigma}_x^{(t)}$, this error is small. However, this regime corresponds to very slow gates and we are here interested instead in the regime in which the corrections to $\hat{\sigma}_x^{(t)}$ have to be taken into account, i.e., $\alpha_\Psi \gtrsim 1$.

The corrected drive strength $\tilde{g} = g/\lambda_c^{\Psi',\Psi}$ accounts for the nonunitary overlap of the motional part of the (dressed)

eigenstates of Eq. (7). These states are displaced Fock states, i.e., $|\Phi\rangle_I = \prod_m \hat{D}(\alpha_{m,\Psi})|n_m\rangle$, which can be produced adiabatically from the Fock states of the noninteracting system. The correction factor $\lambda_c^{\Psi',\Psi}$ is equal to the overlap between the displaced states of any pair of states $|\Psi'\rangle, |\Psi\rangle$. The overlap is dependent on their initial phonon occupation number $|n_m\rangle$ and can be written as [34]:

$$
\lambda_c^{\Psi',\Psi} = \prod_m \langle n_m' | \hat{D}^\dagger(\alpha_{m,\Psi'}) \hat{D}(\alpha_{m,\Psi}) | n_m \rangle
$$
$$
= \prod_m e^{-\beta_m^2/2} \beta_m^{|\Delta n|_m} \left(\frac{n_m!}{n_m'!} \right)^{\text{sign}(\Delta n_m)/2} L_{n_m}^{|\Delta n_m|}(\beta_m^2), \tag{8}
$$

where $\Delta n_m = n_m' - n_m$ and $\beta_m = \alpha_{m,\Psi'} - \alpha_{m,\Psi}$, $L_n^{(\gamma)}(\beta)$ is the associated Laguerre polynomial. Note that the drive strength needed for implementing the correct gate depends therefore explicitly on the motional input state. For the target states in their ground states of motion, $|\Psi_0\rangle, |\Psi_1\rangle$, the overlap simplifies to $\lambda_c^{\Psi_0,\Psi_1} = \prod_m e^{-\beta_m^2/2}$ with $\beta_m = \Omega \eta_m^{(t)}/\delta_m$ and where $L_0(\beta_m^2) = 1$.

C. Adiabatic preparation of states

To guarantee a complete inversion of the target qubit, the system has to be prepared in a nearly pure dressed eigenstate $|\Psi\rangle_I$ of the interacting system such that the drive strength can be exactly corrected using Eq. (8). In the case of a sudden quench (diabatic activation) of Eq. (7), a superposition of dressed eigenstates will result. In contrast, by adiabatic switching (see Appendix A) the qubit-phonon interaction $\hat{H}_{q\text{-ph}}$ and thus $\hat{H}_{\text{Ising}}$, pure (dressed) eigenstates are obtained for which an appropriate drive strength can be chosen.

It also makes our gate robust against residual phonon-qubit entanglement which in turn makes it less sensitive to timing errors. For quenched gates, this residual entanglement occurs if the total gate time $t_T \neq 2k_1\pi/\delta_m$ ($k_1 \in \mathbb{N}$), as in this case the evolution of the states do not describe closed trajectories in phase space. In contrast, the adiabatic ramp assures that the system remains in an eigenstate during the laser-ion interaction. Therefore, the exact timing is not crucial as long as the ramp time is long enough to assure adiabaticity. In practice, however, setting $t_T = 2k_1\pi/\delta_m$ still proves to be useful to reduce errors due to off-resonant drive field coupling between dressed states and to reduce errors caused by nonadiabaticity.

The gate sequence consists then in ramping up the interaction for a time t_a and performing the i-Toffoli gate [Eq. (7)] for a time τ_g, and finally ramp down the interaction to transform the system back to the noninteracting or computational basis. This complete i-Toffoli process has a total length $t_T = 2t_a + \tau_g$ and is described by

$$
\hat{U}_{i\text{Tof}} = \hat{U}_{eg}^d \hat{U}_T \hat{U}_{eg}^a, \tag{9}
$$

where $\hat{U}_{eg}^a$ ($\hat{U}_{eg}^d$) is the unitary of the adiabatic activation (deactivation) of $\hat{H}_{\text{Ising}}$ and $\hat{U}_T = \exp(-i\tau_g \tilde{H}_{T,I})$.

---

[3] In the following we drop the motional component from states in its ground state and label them only by their electronic part, e.g., $|\Psi_0\rangle \rightarrow |0, \vec{x}_c\rangle$.
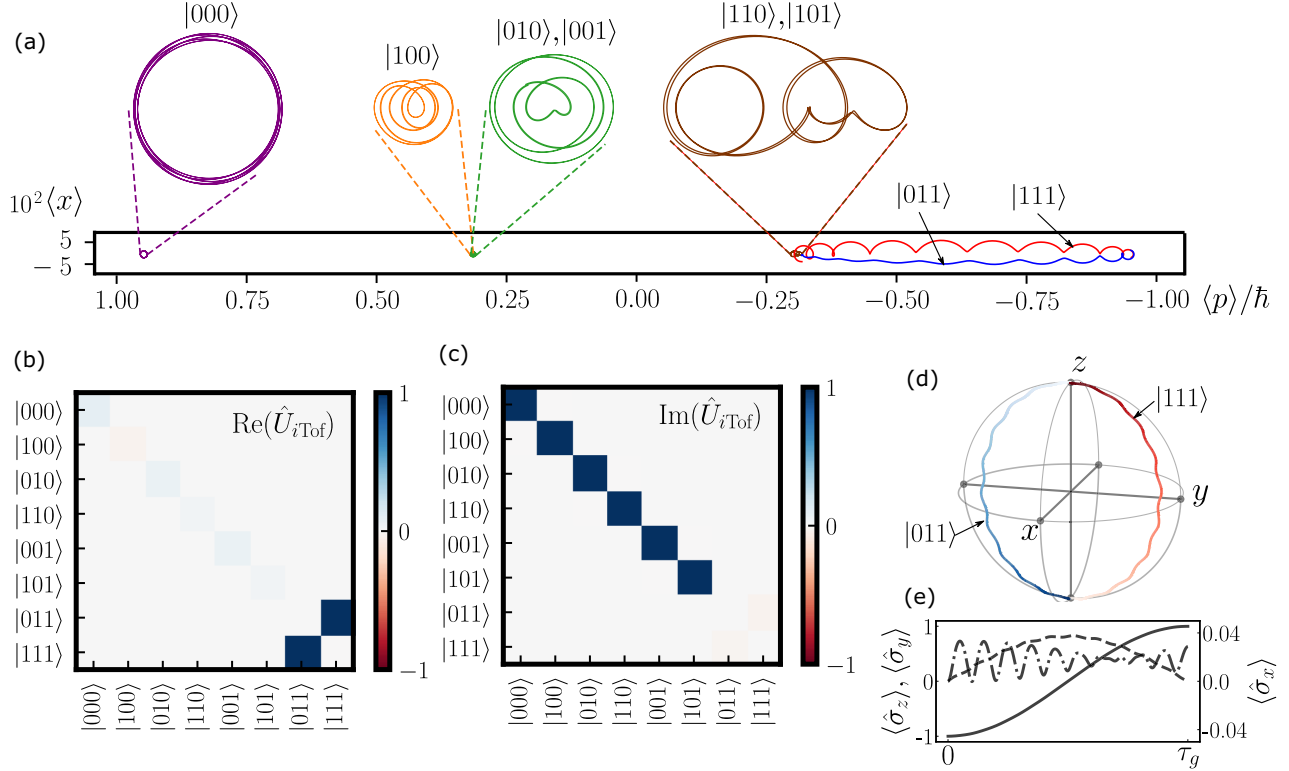
FIG. 2. Time evolution of states under the action of $\tilde{H}_{\mathrm{T,sm}}$ (a) Phase-space trajectories (zoomed in, dimensionless) of motional wave function during evolution with $\hat{U}_{\mathrm{T}}$. Note that the adiabatic ramp ensures that dynamics take place along the momentum axis in this frame, as explained more in detail in Appendix A. (b) Real and (c) imaginary part of process unitary matrix for the motional ground state ($|n=0\rangle$) subspace. (d) Evolution in the Bloch sphere of the two resonant states, and (e) the projections along x ($-\cdot$), y ($--$), and z ($-$) of the trajectory of initial state $|111\rangle$. Time is indicated with the color intensity from light ($t=0$) to dark ($t=\tau_g$) in panel (d). The gate parameters are $\delta_{\mathrm{CM}}/2\pi = 20\,\mathrm{kHz}$, $J/2\pi = 2\,\mathrm{kHz}$ ($\Omega/2\pi = 126.491\,\mathrm{kHz}$), $g/2\pi = 1\,\mathrm{kHz}$ for a gate time of $\tau_g = \pi/g = 500\,\mu\mathrm{s}$.

III. SIMULATIONS OF A *N*-QUBIT TOFFOLI GATE IN A LINEAR ION CRYSTAL

A. Single-mode coupling

The main features of our model can be first studied by considering an ideal system. This consists of a ground-state cooled linear ion crystal and an interaction laser coupling only to the axial modes of the crystal, with a beatnote μ tuned close to the center-of-mass phonon mode frequency ω_{CM} of the crystal, i.e. $\delta_{\mathrm{CM}} \ll \delta_{m \neq \mathrm{CM}}$. We assume that the coupling with the remaining phonon modes can be ignored, i.e., $J_{\mathrm{CM}}^{(i,j)} \gg \sum_{m \neq \mathrm{CM}} J_m^{(i,j)}$. This results in a homogeneous Ising coupling strength $J^{(i,j)} = \Omega^2 \eta_{\mathrm{CM}}^2 / 4\delta_{\mathrm{CM}} \equiv J$ and the simplified Hamiltonian:

$$\tilde{H}_{\mathrm{T,sm}} = 2N_c J \sum_i \hat{\sigma}_z^{(i)} + J \sum_{i \neq j} \hat{\sigma}_z^{(i)} \hat{\sigma}_z^{(j)} + \frac{\tilde{g}}{2} \tilde{\sigma}_x^{(t)} - \delta_{\mathrm{CM}} \hat{a}_{\mathrm{CM}}^\dagger \hat{a}_{\mathrm{CM}}.$$

$$(10)$$

The resulting *i*-Toffoli process unitary for a three-ion crystal is observed in Figs. 2(b) and 2(c). We have chosen a ramp time t_a that ensures the adiabaticity of the process, and the disappearance of dynamical phases. These phases have the form $\phi_{t_\mathrm{T}} = \exp(-iE_{|x_t,\vec{x}_c\rangle} \tilde{t}_\mathrm{T})$, where the total effective process time is $\tilde{t}_T = 2\tilde{t}_a + \tau_g$ and $\tilde{t}_a$ is effective ramp time (see Appendix A). Because the Ising couplings are homogeneous in this particular case, the phases vanish if $\tilde{t}_\mathrm{T} J = 2k_2\pi$ ($k_2 \in \mathbb{N}$). For

a modulation of the form $\Omega(t < t_a) = \Omega \sin^2[\pi t/(2t_a)]$ and these parameters both criteria are fulfilled by setting $t_a = \tau_g$.

To illustrate the dynamics under the action of Eq. (10), we plot the phase space [Fig. 2(a)][4] and Bloch sphere trajectories [Fig. 2(d)] of the (target) dressed states $|\Psi\rangle_\mathrm{I} = \hat{U}_{\mathrm{eg}}^{\mathrm{a}} |n=0\rangle \otimes |x_t, \vec{x}_c\rangle$. As expected for the two target states, the motional and electronic component are transformed from one to the other, i.e., $\hat{D}(\alpha_{\Psi_0})|n=0\rangle \leftrightarrow \hat{D}(\alpha_{\Psi_1})|n=0\rangle$ and $|0,1^2\rangle \leftrightarrow |1,1^2\rangle$. For the off-resonant states, closed trajectories are obtained indicating that motion is disentangled from the electronic component of the states. Finally, in Fig. 2(e) we observe that the coupling of drive with the ion motion, leads to a small drive error reflected as small oscillations of $\langle \hat{\sigma}_x \rangle$.

B. Multimode coupling

In experiments, due to the finite spacing between phonon frequencies, the laser field will couple to multiple phonon modes, as described in Eq. (6). Although the dynamics of the gate will still be dominated by the coupling to the center-of-mass mode, the contributions of nearby modes, $\sum_{m \neq \mathrm{CM}} J_m^{(i,j)}$,

---

[4]The phase space shown in this work is in a rotating frame with frequency μ and the values of $\langle x \rangle$ are in units of the ground-state wave package.
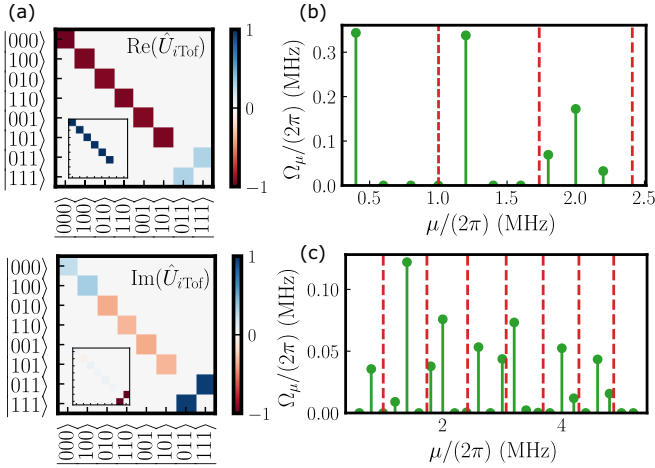
FIG. 3. Multimode unitaries and spectrum of multiple beatnotes for "echo" step for phases cancellation. (a) i-Toffoli unitary for a three-ion crystal considering all-mode couplings without and (inset) with echo step. Frequency and amplitude of beatnotes for (b) three and (c) seven-ion gate with detunings $\delta_{\mathrm{CM}}/2\pi = -20$ kHz and $\delta_{\mathrm{CM}}/2\pi = -50$ kHz, respectively. The phonon mode frequencies are indicated in dashed red lines. The parameters of panel (a) are $\omega_{\mathrm{CM}}/2\pi = 1$ MHz, $\delta_{\mathrm{CM}}/2\pi = -20$ kHz, $g/2\pi = 1$ kHz and for panels (b) and (c) the interaction time is $t_{\mathrm{mb}} = 5\,\mu$s.

will lead to two additional source of errors. The first are additional terms $\propto \alpha_m^{(\mathrm{t})} \hat{\sigma}_y^{(\mathrm{t})}$ which increase the drive error, and the second are state-dependent dynamical phases. The latter occur because the Ising interactions are inhomogeneous, $J^{(i,j)} \neq J^{(i,k)}$, thus the state energies are not longer proportional to a single value of J. As a consequence, no single gate time can be chosen such that they vanish at the end of the gate [Fig. 3(a)].

The first error is minimal if the amplitude of the next-nearest phonon mode at the target ion is close to zero ($\vec{b}_{\mathrm{NN}}^{(\mathrm{t})} \simeq 0$), as in the case of the linear crystal with an odd number of ions and a central target ions. For other configurations, the error can be reduced by increasing spacing between phonon modes, for example, by increasing the trap frequencies. Finally, when reconstructing the Toffoli gate [23], the error is again reduced as the phases on the resonant states are largely suppressed.

To cancel the second error, dynamical phases are reversed with an additional "echo" step. In analogy to a spin echo, the sign of all coupling strengths is inverted $J^{(i,j)} \to -J^{(i,j)}$ for the duration of the gate t_{T}. To realize the inverted couplings required for this echo, we follow a recent proposal [30] in which a combination of multiple beatnotes coupling to all the phonon modes is used to generate couplings with arbitrary magnitude and sign. In short, the method uses beatnotes with frequencies μ_k that are harmonics of the interaction time t_{mb} between the crystal and a multibeatnote laser field, i.e., $\mu_k = 2\pi k/t_{\mathrm{mb}}$ for $k \in \mathbb{N}$. Their amplitudes Ω_{μ_k} [Figs. 3(b) and 3(c)] are calculated such that after a time t_{mb} the entanglement phases accumulated by each of the modes matches a target value φ_m, and in addition both dynamical phases and the entanglement with the phonon modes disappear. The entanglement phases are obtained by expressing the matrix of couplings for the echo step, $\tilde{\mathbf{J}}^{i,j} = -J^{(i,j)}$, in terms of the phonon modes ($\vec{b}_m$)

and the target entanglement phase:

$$\tilde{\mathbf{J}} \cong \sum_{m=1}^{N} \varphi_m \vec{b}_m^{\mathsf{T}} \otimes \vec{b}_m. \tag{11}$$

To reduce the number of beatnotes required, we chose an interaction $t_{\mathrm{mb}} \sim 2k_1\pi/\omega_{\mathrm{CM}}$ for a small integer k_1, that also satisfies $t_{\mathrm{T}} = k_2 t_{\mathrm{mb}}$ ($k_2 \in \mathbb{N}$). This allows for stroboscopically implementing the echo by consecutively applying k_1 multibeatnote field pulses. The amplitudes of the beatnotes Ω_{μ_k} have the same modulation envelope as for the laser-ion coupling strength Ω (see Appendix B).

IV. GATE FIDELITIES AND ERROR SOURCES

We have shown that an i-Toffoli gate ($\hat{U}_{i\mathrm{Tof}}$) can be implemented in a linear crystal of ions in realistic conditions where the effective Ising interaction is generated by coupling to multiple phonon modes of the crystal. In this section, we compare this gate against an ideal i-Toffoli gate ($\hat{U}_{\mathrm{Ideal}}$) for different number of qubits and find conditions for fast gates with high fidelities. Additionally, we are interested in identifying and estimating the effect of other error sources.

To characterize the gate, we use as figure-of-merit the average fidelity $\bar{F}$ [35]:

$$\bar{F}\left(\hat{U}_{i\mathrm{Tof}}, \hat{U}_{\mathrm{Ideal}}\right) = \frac{\sum_j \mathrm{tr}\left[\hat{U}_{\mathrm{Ideal}} U_j^\dagger \hat{U}_{\mathrm{Ideal}}^\dagger \hat{U}_{i\mathrm{Tof}}(U_j)\right] + d^2}{d^2(d+1)},$$
$$\tag{12}$$

where $\hat{U}_{i\mathrm{Tof}}(U_j) \equiv \mathrm{tr}_{\mathrm{FS}}(\hat{U}_{i\mathrm{Tof}}[\hat{P}_0 \otimes U_j]\tilde{U}_{i\mathrm{Tof}}^\dagger)$, U_j are generalized Pauli matrices in the qubit Hilbert space with dimension $d = 2^N$, $\hat{P}_0 = \bigotimes_m |0\rangle\langle 0|_m$ is a projector onto the $n_m = 0$ Fock subspace and $\mathrm{tr}_{\mathrm{FS}}$ is the partial trace of the phonon Fock space.

We start again by assuming single-mode coupling and calculate faster gates by increasing both Ω and g and setting $t_a = \tau_g$ to avoid phase accumulation. By increasing the interaction strengths and reducing gate and ramp times three types of gate errors will have to be accounted for: couplings between off-resonant states, drive errors, and nonadiabatic couplings during ramping of the Ising interaction. To mitigate the first one, we require $J > g$, therefore we keep the ratio $J/g = 2$ for all the gates we will study. The last two errors can be minimized either by extending the duration of the adiabatic ramp or increasing the detuning of the laser beatnote δ_m, both reducing the amplitudes $\alpha_{m,\Psi}$ and thus the final error. Because our goal is a faster gate, we have chosen the latter.

Fidelities higher than 99% with gate times below 500 μs are obtained when $\delta_{\mathrm{CM}}/2\pi = 200$ kHz [Fig. 4(c)] for gates with 3–9 qubits. As a consequence of the reduction of the ramp time with increasing J, the activation of the interaction becomes less adiabatic and the crystal motion is excited. This leads to coupling of motional excited states in the form of $|n > 0\rangle|1, 1^{N_c}\rangle \leftrightarrow |n > 0\rangle|0, 1^{N_c}\rangle$ during the drive step. The larger drops in the fidelity are observed for particular interaction strengths, e.g., $J/4\pi = 3.1$ kHz for $\delta_t/2\pi = 50$ kHz, originate also from undesired couplings between states of the type $|n = 0\rangle \otimes |1, \vec{x}_c\rangle$, $|n = k\rangle \otimes |0, \vec{x}_c\rangle$, which become degenerate when $\Delta_{\vec{x}_c} \sim k\delta_{\mathrm{CM}}$.

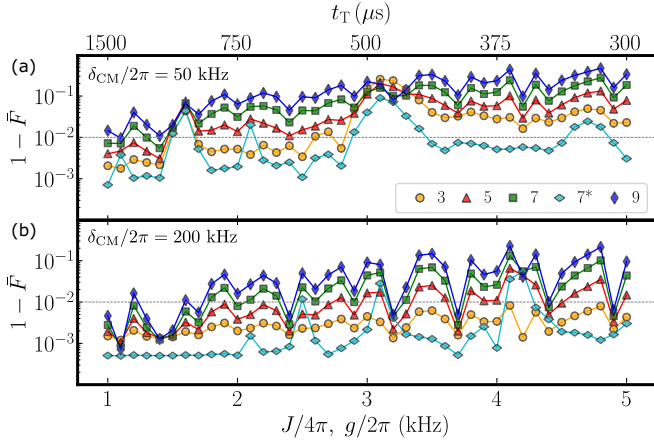These errors affect more strongly gates with larger amount of qubits as the number of states and the occurrence of

FIG. 4. Process error in function of Ising strength and gate time assuming single-mode coupling. The results are for a *i*-Toffoli gate of 3, 5, 7, and 9 ions for detunings of (a) 50, and (b) 200 kHz. We also show the result (7*) for a seven-ion crystal including an "echo" step. In this case, the total process time corresponds to $2t_T$.

degeneracies increases. Furthermore, the drive and nonadiabaticity errors also increase, as the displacement amplitude $\alpha_{m,\Psi} \propto N$. However, by choosing appropriate gate parameters, these undesired couplings can be avoided.

A. Multimode coupling with residual crystal motion

From the single-mode coupling analysis we have identified conditions for high fidelity gates for ion crystals in their ground state. We can use this information to calculate high-fidelity gates for systems where all axial phonon modes participate. We will also take into account residual ion motion such that the average number $\bar{n}_m$ of phonons in the crystal is not zero. In particular, we consider the cases where $\bar{n}_{CM} > 0$ and $\bar{n}_{m \neq CM} = 0$.

To illustrate, we choose gates with the largest detuning ($\delta_{CM}/2\pi = -200$ kHz) to minimize drive errors and select two drive strength values ($g/2\pi = 1.0$; 4.762 kHz) for which no large drop of fidelities were obtained in the single-mode model. As a result, we obtain multimode coupled gates with fidelities better than 99% for both fast [Fig. 5(a)] and slow
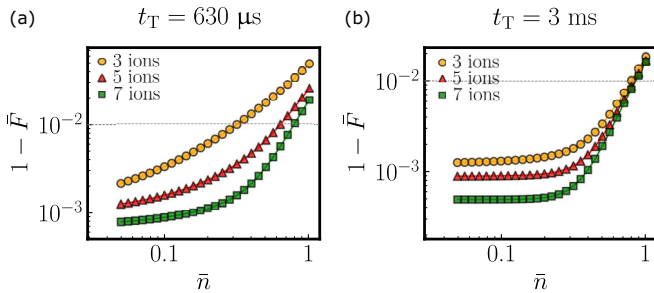

FIG. 5. Effect of average phonon number in process fidelity for gate with multimode coupling. The Ising and drive strengths ($J/4\pi = g/2\pi$) are (a) 4.762 kHz and (b) 1 kHz. The detuning, $\delta_{CM}/2\pi$, and the center-of-mass frequency, $\omega_{CM}/2\pi$, are -200 kHz and 1 MHz, respectively.

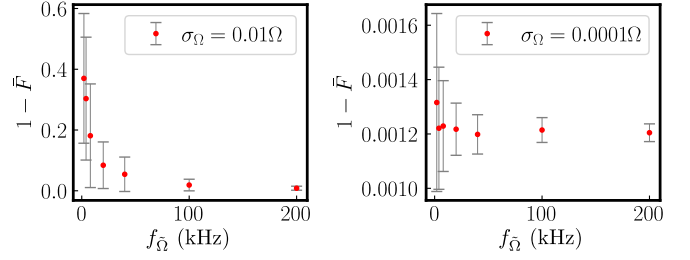

FIG. 6. Gate error for fluctuating Rabi frequency $\tilde{\Omega}$ at frequency $f_{\tilde{\Omega}}$ for two different variances σ_Ω. The gate parameters are $\omega_{CM}/2\pi = 1$ MHz, $\delta_{CM}/2\pi = -200$ kHz, $g/2\pi = 1$ kHz for a gate time of 1500 μs. The results are the average and deviation from 50 realizations.

gates [Fig. 5(b)]. Even in the presence of residual motion up to $\bar{n} = 1$, the fidelities always exceed 90%.

Importantly, the addition of the echo step leads to fidelities that, in most of the cases, are better than those for the single-mode model. Clearly, this step also compensates phases due to Stark shifts originating by couplings of states $|1, \vec{x}_c\rangle \leftrightarrow |0, \vec{x}_c\rangle$, which remained uncorrected in Fig. 4. Moreover, in absence of these phases, higher fidelities are obtained for larger gates (compare with Fig. 4). The increasing gaps between states, $\Delta_{\vec{x}_c}$ for larger systems will reduce any type of off-resonant coupling. In particular, it reduces couplings with excited motional states $\Delta_{\vec{x}_c} \sim k\delta_{CM}$, as the ratio $\Delta_{1_{N_c}}/\delta_m$ increases. Furthermore, not only do these gaps increase, there are also vastly more states with large gaps than with small gaps as N increases. Thus state-specific errors weigh less in the calculation of the average fidelity for larger qubit gates.

Finally, this section provides an indication of the effect of ion heating on the gate fidelity. This an aspect which is present in all ion trap experiments and which requires strict mitigation. For long gate times, in particular, this would lead to incorrect values of the corrected drive strength $\tilde{g}$ which will affect the rotation of the target qubit.

B. Fluctuation of Rabi frequency

A critical aspect of our method is choosing a drive frequency matching the gap between the two resonant states as in Eq. (2). However experimental imperfections could lead to changes of the size of this gap, for example due to fluctuations of the Rabi frequency due to laser intensity instabilities. We analyze this source of error by adding a noise term to the Rabi frequency with variance σ_Ω^2 during the drive step $\hat{U}_T$ (see Appendix C). The effect of the frequency of this noise in the fidelity of a three-ion crystal is shown in Fig. 6. As observed, the gate is severely affected by noise of a timescale of the gate length while the effect decreases at larger frequencies. However, existing and improving techniques should allow the control of this type of noise [36–38].

V. DISCUSSION AND CONCLUSIONS

We have presented a high-fidelity method to implement a single-step *i*-Toffoli gate in trapped ions. Our method allows operating in a regime of strong Ising interactions between qubits, necessary for fast gate operations. Compared with
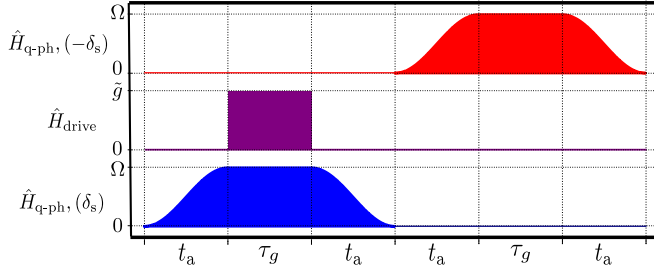
FIG. 7. Strength of Hamiltonian terms during length i-Toffoli gate. The Ising interaction (blue, lower row) is increased before acting with the drive field (purple, middle row) and then lowered again. A "echo" step (red, upper row) can be applied at the end of the gate to correct for residual entanglement or dynamical phases.

the best known gate-based decomposition requiring N^2 CNOT gates [15], thus a quadratic time-scaling, our implementation predicts constant or even improved results with number of qubits at constant gate time. As a result, our gate will suffer less from the accumulation of errors from common sources as motional heating or dephasing, or noise in the optical fields.

We have shown that, when the Ising interactions are mediated by multiple phonon modes, the residual dynamical phases can be effectively removed by using an echo step exploiting a recent nonadiabatic method for multiple qubit entanglement [30]. A natural next step would be to combine our model and this method to generate homogeneous Ising interactions which should allow us to avoid the echo step. As an alternative, the interaction could also be tailored by individual addressing of ions [26], with the drawback of added complexity.

Our method requires high level of control on the preparation of initial states and on the energy spacing between states. In the case of the former, pure phonon states are required to choose the appropriate drive strength $\tilde{g}$, and the latter is necessary to ensure the right drive frequency ω_g and thus an efficient rotation of the target qubit. This sets our implementation apart from a decomposition in, e.g., Mølmer-Sørensen gates [18,19] that are more robust with respect to the phonon states [17,39] and show no sensitivity to a drive frequency. On the other hand, pure phonon states can be assured by well-established ground state cooling techniques and additional methods [40] are available to minimize the effect of heating during gate operations. For the control of the energy gap, laser intensity stabilization with subpercentage noise will be required.

Finally, our proposal could be combined with recent methods of shortcut to adiabaticity [41–43] to speed up the adiabatic preparation of states and reduce the gate time.
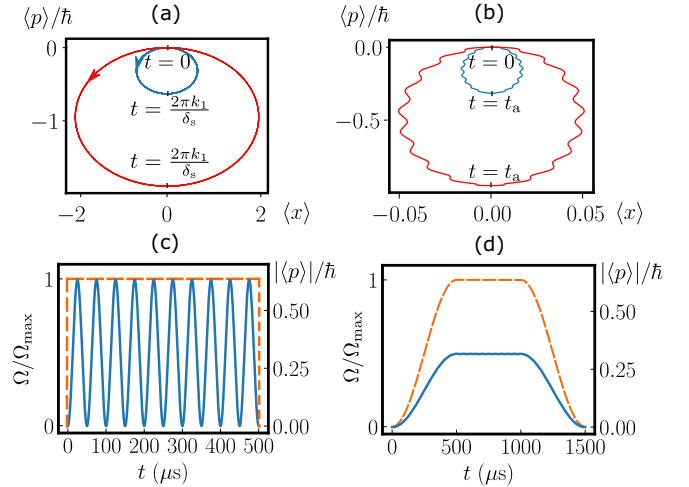
ACKNOWLEDGMENTS

FIG. 8. Phase-space trajectories (dimensionless) of target states under the application of $\hat{H}_{\text{q-ph}}$. Trajectories of $|111\rangle$ (red, outer trajectory) and $|011\rangle$ (blue, inner trajectory) wave packages and evolution of momentum expectation value (blue, solid line) of $|011\rangle$ due to (a), (c) a quench activation of 500 μs and (b), (d) an adiabatic modulation of $\hat{H}_{\text{q-ph}}$ (orange, dashed line). $\langle x \rangle = 0$ at the times indicated in panels (a) and (b).

APPENDIX A: MODULATION OF ISING INTERACTION

The adiabatic transformation between the noninteracting and dressed states basis is realized by slowly increasing (decreasing) the strength of the Ising interaction for a time $t_a \gg 1/\delta_s$. This is achieved by modulating the Rabi frequency of the laser-ion Hamiltonian $\hat{H}_{\text{q-ph}}$, such that $\Omega(t) = \Omega \sin^2(\frac{\pi}{2} t/t_a)$ for $t < t_a$ and $\Omega(t') = \Omega \cos^2(\frac{\pi}{2} t'/t_a)$ with $t' = t - t_a - \tau_g$ for $t > t_a + \tau_g$ (Fig. 7). As a result we obtain the time-dependent Ising couplings $J(t) \propto \Omega(t)^2$. This modulation leads to a pulse area equivalent to that of a square pulse of half the length, such that we define an effective ramp time as $\tilde{t}_a = 0.5 t_a$.

As seen in Figs. 8(a) and 8(b), the displacement in phase space of the two target states are significantly reduced for the adiabatically initialized system. This minimizes errors due to the noncommutativity between the drive and Ising interaction fields and also those arising from residual phonon-qubit coupling. To approximate the unitary evolution of this adiabatic process we use a Trotter-Suzuki expansion:[5]

$$\hat{U}_{\text{eg}}^{\text{a}} = \prod_{t=0}^{t_a} e^{-i\Delta t \hat{H}_{\text{Ising}}(t)} e^{-i\Delta t \tilde{H}_0},$$

$$\hat{U}_{\text{eg}}^{\text{d}} = \prod_{t=t_a}^{0} e^{-i\Delta t \hat{H}_{\text{Ising}}(t)} e^{-i\Delta t \tilde{H}_0}, \tag{A1}$$

where

$$\hat{H}_{\text{Ising}}(t) = J(t) \sum_{i \neq j} \hat{\sigma}_z^{(i)} \hat{\sigma}_z^{(j)}, \tag{A2}$$

$$\tilde{H}_0 = 2 N_c J(t_a) \sum_i \hat{\sigma}_z^{(i)} - \delta_s \hat{a}_s^\dagger \hat{a}_s, \tag{A3}$$

---

[5]$[\hat{H}_{\text{Ising}}, \hat{H}_0] \neq 0$.

and $\Delta t \ll (1/k)\delta_s \ll t_a$ is the time-step of the expansion and $k = t_a \delta_t / 2\pi$.

APPENDIX B: ELIMINATION OF RESIDUAL ENTANGLEMENT AND DYNAMICAL PHASES

Whenever the timing condition for the elimination of dynamical phases, $\tilde{t}_T J = 2k_2\pi$, is not fulfilled, it is possible to add an additional echo step to the process to correct for these errors (Fig. 7). In this step the sign of the interaction strength is also reversed, i.e., $J \to -J$. For the single-mode coupling model, this is obtained by inverting the sign of the detuning $\delta_s \to -\delta_s$. In the case of multimode coupling, we have used a combination of multiple beatnotes to generate an effective Ising interaction reversing the sign of the couplings during the gate step. More details of this method can be found in Ref. [30].

The modulation of the coupling strengths between the ion and the single Ω or multimode laser fields Ω_{μ_k} is equal to

the one during the application of the initial gate. Furthermore, the length of the step needs also to be equal to total process time t_T and during the constant coupling strength portion of the echo, no drive field is applied. In summary, this step can be described by the unitary

$$\hat{U}_{SE} = \hat{U}_{eg}^a \hat{U}_I \hat{U}_{eg}^d, \tag{B1}$$

where $\hat{U}_I = e^{-it\tau_g[\hat{H}_{Ising}(t_a) + \tilde{H}_0]}$ and the signs of $J(t)$ and δ_s are inverted in the Hamiltonians $\hat{H}_{Ising}(t)$ and $\tilde{H}_0$.

APPENDIX C: EVOLUTION WITH A NOISY GATE

To introduce a fluctuation on the Rabi frequency during the gate, we calculate the $\hat{U}_T$ as $\hat{U}_T = \prod_i^S \exp(-i\Delta\tau_g \tilde{H}_{T,I,\tilde{\Omega}})$, where $\Delta\tau_g = \frac{1}{f_{\tilde{\Omega}}}$, $S = \tau_g f_{\tilde{\Omega}}$, $\tilde{H}_{T,I,\tilde{\Omega}}$ corresponds to the Hamiltonian of Eq. (7) with a fluctuating Ising coupling $J_{\tilde{\Omega}} = \tilde{\Omega}^2 \sum_m \eta_m^{(i)} \eta_m^{(j)} / 4\delta_m$ and $\tilde{\Omega}$ is sampled from a normal distribution with mean Ω and standard deviation σ_Ω.

[1] S. P. Jordan, K. S. M. Lee, and J. Preskill, Quantum algorithms for quantum field theories, Science **336**, 1130 (2012).

[2] A. Aspuru-Guzik, A. D. Dutoi, P. J. Love, and M. Head-Gordon, Simulated quantum computation of molecular energies, Science **309**, 1704 (2005).

[3] D. S. Abrams and S. Lloyd, Quantum Algorithm Providing Exponential Speed Increase for Finding Eigenvalues and Eigenvectors, Phys. Rev. Lett. **83**, 5162 (1999).

[4] P. Jaksch and A. Papageorgiou, Eigenvector Approximation Leading to Exponential Speedup of Quantum Eigenvalue Calculation, Phys. Rev. Lett. **91**, 257902 (2003).

[5] D. A. Lidar and H. Wang, Calculating the thermal rate constant with exponential speedup on a quantum computer, Phys. Rev. E **59**, 2429 (1999).

[6] J. Zhang, G. Pagano, P. W. Hess, A. Kyprianidis, P. Becker, H. Kaplan, A. V. Gorshkov, Z.-X. Gong, and C. Monroe, Observation of a many-body dynamical phase transition with a 53-qubit quantum simulator, Nature (London) **551**, 601 (2017).

[7] F. Arute, K. Arya, R. Babbush, D. Bacon, J. Bardin, R. Barends, R. Biswas, S. Boixo, F. Brandao, D. Buell, B. Burkett, Y. Chen, J. Chen, B. Chiaro, R. Collins, W. Courtney, A. Dunsworth, E. Farhi, B. Foxen, A. Fowler *et al.*, Quantum supremacy using a programmable superconducting processor, Nature (London) **574**, 505 (2019).

[8] C. Figgatt, D. Maslov, K. A. Landsman, N. M. Linke, S. Debnath, and C. Monroe, Complete 3-qubit grover search on a programmable quantum computer, Nat. Commun. **8**, 1918 (2017).

[9] V. Vedral, A. Barenco, and A. Ekert, Quantum networks for elementary arithmetic operations, Phys. Rev. A **54**, 147 (1996).

[10] S. A. Cuccaro, T. G. Draper, S. A. Kutin, and D. P. Moulton, A new quantum ripple-carry addition circuit, arXiv:quant-ph/0410184.

[11] R. Van Meter and K. M. Itoh, Fast quantum modular exponentiation, Phys. Rev. A **71**, 052320 (2005).

[12] A. Paetznick and B. W. Reichardt, Universal Fault-Tolerant Quantum Computation with only Transversal Gates and Error Correction, Phys. Rev. Lett. **111**, 090505 (2013).

[13] L. K. Grover, A fast quantum mechanical algorithm for database search, in *Proceedings of the Twenty-Eighth Annual ACM Symposium on Theory of Computing, STOC'6* (Association for Computing Machinery, New York, 1996), pp. 212–219.

[14] D. Maslov and G. W. Dueck, Improved quantum cost for *n*-bit Toffoli gates, Electron. Lett. **39**, 1790 (2003).

[15] V. V. Shende and I. L. Markov, On the CNOT-cost of TOFFOLI gates, Quantum Info. Comput. **9**, 461 (2009).

[16] N. M. Linke, D. Maslov, M. Roetteler, S. Debnath, C. Figgatt, K. A. Landsman, K. Wright, and C. Monroe, Experimental comparison of two quantum computing architectures, Proc. Natl. Acad. Sci. USA **114**, 3305 (2017).

[17] A. Sørensen and K. Mølmer, Quantum Computation with Ions in Thermal Motion, Phys. Rev. Lett. **82**, 1971 (1999).

[18] D. Maslov and Y. Nam, Use of global interactions in efficient quantum circuit constructions, New J. Phys. **20**, 033018 (2018).

[19] K. Groenland, F. Witteveen, K. Schoutens, and R. Gerritsma, Signal processing techniques for efficient compilation of controlled rotations in trapped ions, New J. Phys. **22**, 063006 (2020).

[20] L. Isenhower, M. Saffman, and K. Mølmer, Multibit C_k NOT quantum gates via Rydberg blockade, Quantum Inf. Process. **10**, 755 (2011).

[21] M. Khazali and K. Mølmer, Fast Multiqubit Gates by Adiabatic Evolution in Interacting Excited-State Manifolds of Rydberg Atoms and Superconducting Circuits, Phys. Rev. X **10**, 021054 (2020).

[22] K. Mølmer, L. Isenhower, and M. Saffman, Efficient grover search with Rydberg blockade, J. Phys. B: At., Mol. Opt. Phys. **44**, 184016 (2011).

[23] S. E. Rasmussen, K. Groenland, R. Gerritsma, K. Schoutens, and N. T. Zinner, Single-step implementation of high-fidelity *n*-bit Toffoli gates, Phys. Rev. A **101**, 022308 (2020).

[24] D. Leibfried, B. DeMarco, V. Meyer, D. Lucas, M. Barrett, J. Britton, W. M. Itano, B. Jelenković, C. Langer, T. Rosenband, and D. J. Wineland, Experimental demonstration of a robust, high-fidelity geometric two ion-qubit phase gate, Nature (London) **422**, 412 (2003).

[25] C. F. Roos, Ion trap quantum gates with amplitude-modulated laser beams, New J. Phys. **10**, 013002 (2008).

[26] K. Kim, M.-S. Chang, R. Islam, S. Korenblit, L.-M. Duan, and C. Monroe, Entanglement and Tunable Spin-Spin Couplings between Trapped Ions Using Multiple Transverse Modes, Phys. Rev. Lett. **103**, 120502 (2009).

[27] C. J. Ballance, T. P. Harty, N. M. Linke, M. A. Sepiol, and D. M. Lucas, High-Fidelity Quantum Logic Gates Using Trapped-Ion Hyperfine Qubits, Phys. Rev. Lett. **117**, 060504 (2016).

[28] J. P. Gaebler, T. R. Tan, Y. Lin, Y. Wan, R. Bowler, A. C. Keith, S. Glancy, K. Coakley, E. Knill, D. Leibfried, and D. J. Wineland, High-fidelity Universal Gate Set for ^{9}Be$^+$ Ion Qubits, Phys. Rev. Lett. **117**, 060505 (2016).

[29] N. Goel and J. K. Freericks, Native multiqubit Toffoli gates on ion trap quantum computers, arXiv:2103.00593.

[30] Y. Shapira, R. Shaniv, T. Manovitz, N. Akerman, L. Peleg, L. Gazit, R. Ozeri, and A. Stern, Theory of robust multi-qubit non-adiabatic gates for trapped-ions, Phys. Rev. A **101**, 032330 (2020).

[31] D. Porras and J. I. Cirac, Effective Quantum Spin Systems with Trapped Ions, Phys. Rev. Lett. **92**, 207901 (2004).

[32] X.-L. Deng, D. Porras, and J. I. Cirac, Effective spin quantum phases in systems of trapped ions, Phys. Rev. A **72**, 063407 (2005).

[33] I. G. Lang and Y. A. Firsov, Calculation of the activation probability for a jump of a small-radius polaron, J. Exp. Theor. Phys. **27**, 443 (1968).

[34] K. E. Cahill and R. J. Glauber, Ordered expansions in boson amplitude operators, Phys. Rev. **177**, 1857 (1969).

[35] M. A. Nielsen, A simple formula for the average gate fidelity of a quantum dynamical operation, Phys. Lett. A **303**, 249 (2002).

[36] F. Tricot, D. H. Phung, M. Lours, S. Guérandel, and E. de Clercq, Power stabilization of a diode laser with an acousto-optic modulator, Rev. Sci. Instrum. **89**, 113112 (2018).

[37] J. Junker, P. Oppermann, and B. Willke, Shot-noise-limited laser power stabilization for the AEI 10 m prototype interferometer, Opt. Lett. **42**, 755 (2017).

[38] L. Duan, J. Fang, R. Li, L. Jiang, M. Ding, and W. Wang, Light intensity stabilization based on the second harmonic of the photoelastic modulator detection in the atomic magnetometer, Opt. Express **23**, 32481 (2015).

[39] G. Kirchmair, J. Benhelm, F. Zähringer, R. Gerritsma, C. F. Roos, and R. Blatt, Deterministic entanglement of ions in thermal states of motion, New J. Phys. **11**, 023002 (2009).

[40] M. Cetina, L. N. Egan, C. A. Noel, M. L. Goldman, A. R. Risinger, D. Zhu, D. Biswas, and C. Monroe, Quantum gates on individually-addressed atomic qubits subject to noisy transverse motion, arXiv:2007.06768.

[41] S. An, D. Lv, A. del Campo, and K. Kim, Shortcuts to adiabaticity by counterdiabatic driving for trapped-ion displacement in phase space, Nat. Commun. **7**, 12999 (2016).

[42] A. Baksic, H. Ribeiro, and A. A. Clerk, Speeding up Adiabatic Quantum State Transfer by Using Dressed States, Phys. Rev. Lett. **116**, 230503 (2016).

[43] T. Yan, B.-J. Liu, K. Xu, C. Song, S. Liu, Z. Zhang, H. Deng, Z. Yan, H. Rong, K. Huang, M.-H. Yung, Y. Chen, and D. Yu, Experimental Realization of Nonadiabatic Shortcut to Non-Abelian Geometric Gates, Phys. Rev. Lett. **122**, 080501 (2019).